HAILO: A Sensorised Hand Splint for the Exploration of Interface Forces

Dominic Jones, *Member, IEEE*, Vasiliki Vardakastani; Angela E. Kedgley; Matthew D. Gardiner;
Tonia L. Vincent; Peter R. Culmer, *Member, IEEE*, and Ali Alazmani[*], *Member, IEEE*

Abstract— **This study presents the design and development of an instrumented splint for measuring the biomechanical effects of hand splinting and for assessing interface loading characteristics for people with arthritis. Sixteen multi-axial soft load-sensing nodes were mounted on the splint-skin interface of a custom 3D printed thumb splint. The splint was used to measure the interface forces between splint and hand in 12 healthy participants in 6 everyday tasks. Forces were compared between a baseline relaxed hand position and during states of active use. These data were used to generate a measure of sensor activity across the splint surface. Through direct comparison with a commercial splint, the 3D printed splint was deemed to provide similar levels of support. Observation of the activity across the 16 sensors showed that 'active' areas of the splint surface varied between tasks but were commonly focused at the base of the thumb. Our findings show promise in the ability to detect the changing forces imparted on the hand by the splint surface, objectively characterising their behaviour. This opens the opportunity for future study into the biomechanical effects of splints on arthritic thumbs to improve this important intervention and improve quality of life.**

Index Terms—**Soft Sensor, Multi-axial Force Sensor, Instrumented Splint, Soft Robotics, Hall-Effect Sensor**

I. INTRODUCTION

As a consequence of the ageing population, cases of arthritis are rising. First carpometacarpal (CMC1) arthritis is a painful disease presenting with pain at the base of the thumb. The prevalence of the disease varies with age and gender, with post-menopausal women the most affected at 33% [1]–[3]. Despite this, the condition is often not reported to doctors and therefore goes untreated [4]. As little as 4% of patients seek treatment after diagnosis [5], with many patients accepting the pain as a part of life. The CMC1 joint of the thumb (see Fig. 1a) is notable within the body as one of only two saddle joints. The reciprocally curved concave-convex articular surfaces allow for two degrees of freedom, permitting rotations in flexion/extension and adduction/abduction [6]. This freedom allows for circumduction of the thumb and assists in thumb opposition. The CMC1 joint has an inherent instability, a consequence of the increased range of motion. The concave
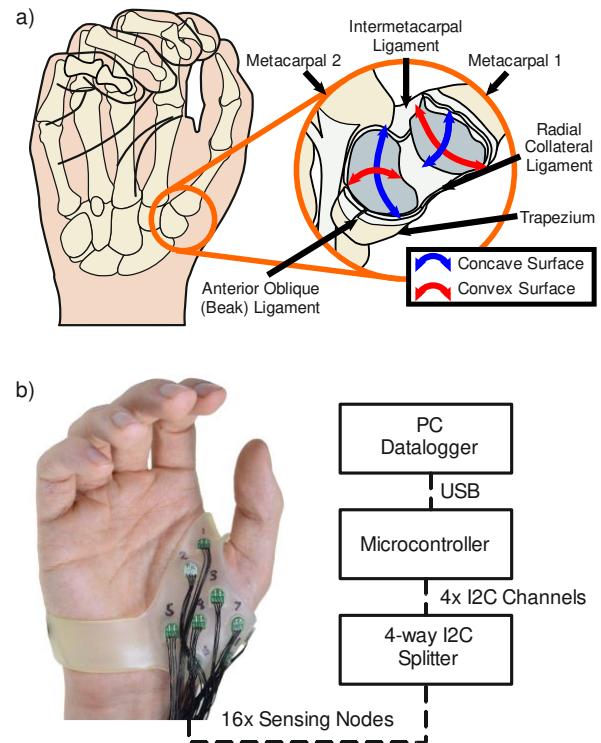
Fig. 1. a) The first carpometacarpal joint, indicating the concave-convex faces of the saddle joint. b) HAILO system concept, 16 sensing nodes in a thumb splint

joint face is shallow and has no surrounding bony structures to stabilise the joint, leading to an increased risk of CMC1 arthritis [7], [8].

While there is no known cure for CMC1 arthritis, many treatments are available to patients which aim to provide symptomatic relief, with options of surgery available for the more advanced cases [5]. Nonsurgical treatment options focus on preventing and managing patient pain and are typically used in the earlier stages of the disease. The primary techniques are behaviour management (preventing actions that cause aggravation) and splinting to prevent movement of the thumb and offload the joint. To relieve pain nonsteroidal anti-inflammatory medications may be prescribed, with intra-articular corticosteroid injection used in more severe cases.

For CMC1 arthritis, clinicians commonly prescribe splints to offload and restrict the first metacarpal bone movement [9], allowing freedom of movement for all other joints in the hand [10]. The movement restriction stabilises the joint and prevents subluxation of the CMC joint during pinch actions, reducing the

pain caused by high joint stresses [11]. Studies have shown improvements in hand function and reduced pain [12], [13], but no significant difference has been found between splinting types [14]–[16]. This has led to a questioning of the clinical effectiveness of splints due to a paucity of information on the subject [17], [18], as some commonly used splints offer little-to-no mechanical support to the joint. This highlights a need for improved understanding of splint mechanics and an opportunity to use sensing technology to assess this through measurement of the splint-hand interaction forces.

To date, there has been little reported use of force sensing in hand splints. Of the few examples, a device used by Giesberts *et al.* [19], [20] used a single axis inductive force sensor to measure the variance of interface force in a hand splint for Dupuytren Contracture. A single-axis force sensor (10 mm diameter) was placed adjacent to an affected metacarpophalangeal or proximal interphalangeal joint. This sensor measured tissue contact pressures on the finger of up to 7 kPa. Cha *et al.* introduced a commercial pressure sensing pad between the skin and a carpal tunnel splint to assess pressure distributions between the hand and splint. The device aimed to detect regions of high pressure on the palmar hand in order to assist splint usage. Pressures of up to 20 kPa were observed, focusing around the palmar base of the thumb. While this gives an insight into pressure magnitude and localisation in a hand splint, they would likely vary due to the different geometry of the thumb spica. Xinyang *et al.* produced a 3D force-sensing skin to measure contact pressures between a patient and a hand/wrist orthosis [21]. The skin wrapped around the patient's hand, with the splint worn over the top. Contact pressures between 20 to 78 kPa were observed across the interface on a single participant. Twelve custom resistive sensors were placed in areas likely to experience high pressures, deduced by finite element simulation. This simulation indicated an area of high pressure in the area above the CMC1 joint, showing the importance of contact forces around this area.

To address the challenge of instrumenting a hand splint, several key requirements must be addressed. Firstly, determining what to measure is challenging given the limited research to date. However, valuable information can be learned from passive orthotic devices with similar mechanisms. Devices to measure interface forces and pressures can be found in plaster casts [22], [23], prosthesis sockets [24], [25], chest braces [26] and insoles [27], [28]. Among these devices, many focus on introducing an array of force sensing nodes within the device-skin interface. Input forces vary owing to the different locations of the device. In addition, shear forces at the device interface are indicated to be important to clinical function, an aspect that typically involves bespoke measurement technology [29], [30].

Another key requirement is a sensing approach with conformability to the human body. For a splint, this should allow contact between the sensor and hand through different positions, assisting with the validity of measurement. Commercial force sensing technologies are typically either solid load-cell or thin-film packages, which will not conform to the hand. A soft sensor based on silicone elastomer is soft enough to deform and follow the skin without altering splint function [31]. Our previous work has produced a three-axis soft tactile sensor capable of measuring pressures typical of that in

an upper limb splint-skin interface [32]. These sensors have indicated their usefulness in an adapted commercial splint; however, limitations were observed in their spatial resolution.

In this work, we aim to produce a sensorised thumb splint to enable the exploration of splint-hand interaction loads (Fig. 1b). This paper details the creation and validation of the splint using three-axis soft tactile sensing technology based on the Hall-Effect to detect the varying pressure and shear at the splint-hand interface. The system is demonstrated in a twelve-participant pilot study, in which the variation of splinting forces during everyday tasks is recorded. From this, we assess the areas in the splint which hold greater importance when it comes to force sensing, which may inform future splint design and functionality or any underlying biomechanical interactions.

II. MATERIALS AND METHODS

Thumb splints used for CMC1 arthritis typically wrap around the thumb, with a strap around the palm to fix the splint in place. We aim to apply tactile sensing to the inner face to assess the mechanical forces imparted on the thumb. The soft tactile sensors consisted of three main components: a three-axis Hall-effect sensor, a silicone elastomer, and a neodymium magnet. Under load, the elastomer deforms, displacing the magnet and varying a measured magnetic field vector. This change in field strength may be calibrated to force. To achieve sensing in the
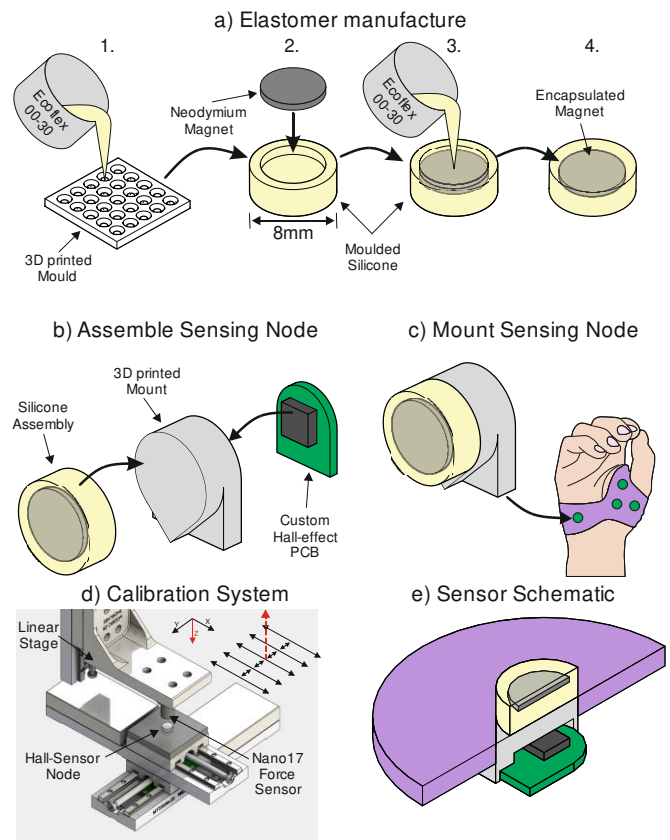
Fig. 2. a) Manufacturing process for the sensing nodes. A 6 × 0.5 mm magnet is embedded within an 8 × 3 mm cylinder of moulded silicone elastomer (Ecoflex 00-30). b) The sensor PCB is attached to a 3D printed mount. The elastomer is affixed to the front face of the mount to complete the sensor. c) Individual sensing nodes are mounted to the splint in specified positions. d) The calibration system; inset: diagram of the positional change for the calibrations sweep. e) The manufactured sensor placed through the splint surface

splint skin interface, we attached several sensing nodes to the hand splint's internal face.

In this work, we inserted these sensors into a commercial thumb splint (Push Ortho Thumb Brace, Nea International bv, Netherlands); however due to structural components of the splint, the location and spatial resolution of the sensors were limited. To remedy this, a 3D printed splint was designed and fabricated with a similar geometry but the flexibility to freely integrate sensor elements in high density across the skin interface. The custom splint was checked against the commercial splint for parity in baseline pressure measurements before wider evaluation in the pilot study reported in Section II-D.

A. Sensor Node Design

To measure the three-axis contact forces across the inside surface of the splint an array of 16 soft tactile sensors was integrated. These sensors, based on a previous concept by Wang *et al.* [33], were developed and characterised in our previous work [32] to increase sensitivity at a reduced size. The electronics of the sensor were also miniaturised, reducing their size to 7×6 mm to increase the special density of sensors on the splint surface. The elastomer layer of the sensor was an 8×3 mm disc of Ecoflex 00-30, with a 6×0.5 mm neodymium magnet embedded. This layer thickness ensured constant contact with the skin in the stiffer 3D printed splint. To ensure the sensors operated within the typical pressure range in the splint-skin interface, the calibration ranges of the sensors were set to stresses of 45 kPa normal and 6 kPa shear. Our previous work provides further details on the sensor and its design parameters [32]. The manufacturing process of the sensor nodes is presented in Fig. 2.

Owing to the complex, non-linear nature of the relationship between the measured magnetic field vector ($\mathbf{B}$) and applied force vector ($\mathbf{F}$), neural network fitting has been used to discern the calibration between the two. Our previous works have used similar fitting methods for similarly non-linear systems [32]. The fitting generates equation 1.

$$\mathbf{F} = f_1(\mathbf{B}) \tag{1}$$

Previous iterations of the Hall-effect based tactile sensor have indicated that this single calibration is insufficient for usage when many sensors are required to be calibrated at once. In these previous cases, manufacturing error caused incorrect placement of the magnet such that its initial displacement was not equal to zero. As this offset changed, the overall relationship between $\mathbf{B}$ and $\mathbf{F}$ also changes, leading to the need for individual calibrations per sensor.

To rectify this, we propose a two-step calibration method where the equation, f_1, is split into two separate equations, between which the magnet offset ($\mathbf{d}$) is tared by the initial magnet offset ($\mathbf{d}_0$). The updated calibration process is described in equations 2 & 3.

$$\mathbf{d} = f_2(\mathbf{B}) \tag{2}$$

$$\mathbf{F} = f_3(\mathbf{d} - \mathbf{d}_0) \tag{3}$$

This modification allows manufacturing discrepancies to be nullified after the first stage of the equation. In this way, the function f_2 would only vary with changes to the magnet parameters and function f_3 with changes to the elastomeric material.

A three-axis loading setup [29], [32] (Fig. 2d) was used to generate training data. First, we generated training data for the magnet position by moving a 6×0.5 mm magnet in a $4 \times 4 \times 4$ mm matrix above a three-axis Hall-effect sensor. This recorded the relationship between magnetic field and displacement. Next, the same platform applied load to three manufactured sensors in normal and both shear directions using applied displacement. From our previous work, the maximum expected displacement under load was 1 mm d_z and 0.3 mm in d_x and d_y. For the calibration, the sensor was indented to 2 mm d_z and 0.6 mm in d_x and d_y. We recorded data from multiple sensors to account for manufacturing discrepancies between the sensors, allowing for the generation of a displacement-force relationship specific to the sensor geometry and material; rather than individual sensor assemblies.

Neural networks were used to generate calibration functions (f_2 and f_3) for the complex relationships from both B-to-d and d-to-F. The networks were trained using the MATLAB Neural Network Fitting toolbox (r2019a, Mathworks Inc., MA, USA). Two-layer feed-forward networks were trained, with ten neurons in the hidden layer and an inverse tangent activation function. The network training specification was chosen to mirror our other works on soft tactile sensing [34].

The sensors were tested dynamically to assess the effects of the new calibration, as well as the hysteresis and creep errors induced by the non-linear material response of the elastomer layer (presented in Fig. 3). Three sensors were indented to 1 mm in Z, and 0.3 mm in X and Y simultaneously. For Hysteresis error, a sensor was indented as above, and was repeated 5 times. The hysteresis error in the sensor was 5% in F_z, and 5% in F_x and F_y. The sensor's error between loading was 0.1% in each axis. For creep testing, the sensor was loaded as above, 5 times. The sensor was held in the loaded position for
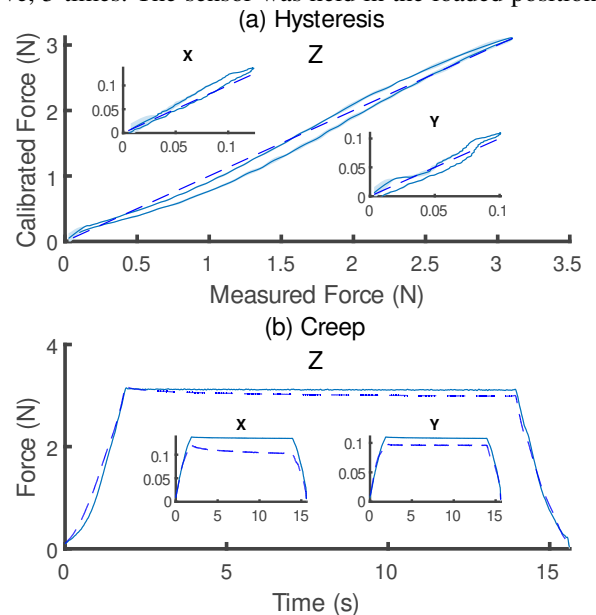

Fig. 3. Mean response of three sensor nodes (STD represented by shaded error region): a) Hysteresis of the sensor node. b) Creep response of the sensor nodes

12 s before releasing. Over the 12 s, creep induced error was observed to be 3% in F_z, and 20% in F_x and 10% in F_y.

The sensors are prone to crosstalk due to the permanent magnets used as a transducer mechanism. Because of this, a minimum separation distance was defined that was intrinsic to the design of the splint. In our previous design analysis of the sensors [32], a minimum sensor separation distance of 12 mm was selected, which allowed for a dissipation of the field between magnets down to 100 times the magnitude of the 'Earth's magnetic field, or 1 % of the maximum sensing range. This allowed for a total of four sensors to be integrated into the commercial splint, and 16 sensors in the 3D printed splint.

B. Instrumented Commercial Splint

Using sensor designs based on our previous work [31], we integrated four sensing nodes within a commercially available thumb splint. As shown in Fig. 4a, the sensors were located at intervals around the circumference of the thumb. Other placement locations are limited by a metal plate embedded within the splint to provide additional stiffness. With this limited space, in addition to the minimum sensor separation constraint of 12 mm, led to the addition of a maximum of four sensors. Retroactively fitting sensors into the commercial splint design also made it challenging to precisely control the final orientation of the sensor relative to the splint surface.

C. Instrumented 3D Printed Splint

3D printing the splint body offered a solution to precise positioning and alignment of sensor nodes. The position and desired alignment of the sensors were integrated into the splint body by creating recesses for each node during the 3D design process and prior to fabrication. To maintain consistency with the instrumented commercial splint, we used a 3D scanner (Spider, Artec3D, Luxembourg) to reproduce the geometry of the commercial thumb splint, before orienting and cutting recess geometries from the model. To allow comparison of measured data between the commercial and 3D printed splints, we replicated the four sensor node locations from the commercial splint design and added 12 additional sensor node locations to fully populate the splint surface. The replicated sensor nodes were numbered: 1, 7, 10 and 15. We then compared the loading at these locations between splints, firstly to check the baseline fit and secondly to check the forces under a functional task (a tripod grip).

D. Validation Experiment

1) Participants

12 healthy participants were recruited. Participants were eligible if they did not have any disease that would negatively affect hand function. Participants were 30±5 years old, with a mean hand circumference of 21.4±0.7 cm. Ethical approval was provided by the University of Leeds Research ethics committee (Ref: MEEC 19-017 – HAILO; Granted: 05/06/2020) and all participants provided informed written consent for data to be recorded.

2) Measurement Protocol

All participants were seated in front of a table and asked to sign the study documents. After this, the participant's hand circumference was recorded. The hand circumference was measured around the hand, 2nd to 5th metacarpophalangeal joints. Each participant had the prototype 3D printed splint fitted to their right hand, with all trailing wires routed along the wrist and forearm. Once the splint was fitted, the participant asked to open and close their hand 10 times, to allow the splint to settle on to the hand. They were then asked to perform a series of functional tasks designed to replicate everyday activities: a bottle raise, jar twist, key turn, and foam grasp (Fig. 5). Two typical grips were tested on the foam grasp: a tripod grip and pinch grip. Further details on the functional tasks are provided in Appendix A.
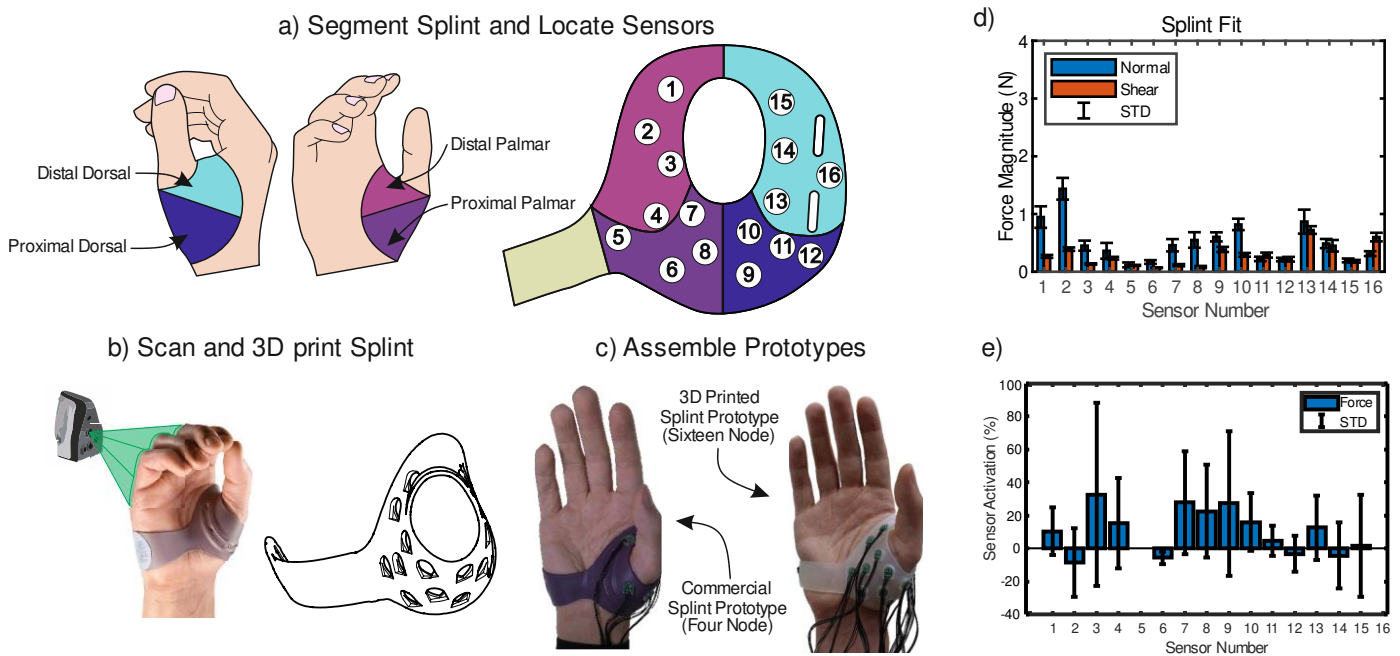
Fig. 4. The prototyping procedure of the 3D printed prototype splint: a) The thumb base is segmented into four zones. The sensors are then located across the splint face; b) The commercial splint is scanned, spaced for sensors cut, and then 3D printed; c) The sensors are attached around the face of the splint, with positions marked on the schematic. d) An example of mean force magnitudes in normal and shear across a single task; e) Observed mean sensor activation

Fig. 5. Tasks performed in the healthy trial with an example force trace: a) Bottle Lifts, b) Jar Open, c) Foam Squeeze, and d) Key Turn

A glass bottle (diameter 66 mm, height 245 mm) was used for the bottle raise and was weighted with water to 350, 600, and 850 g. Participants were asked to grasp the bottle with a cylinder grip, and lift 10 cm from the table, and replace it in the same marked space. To ensure that forces were not measured from direct contact between the bottle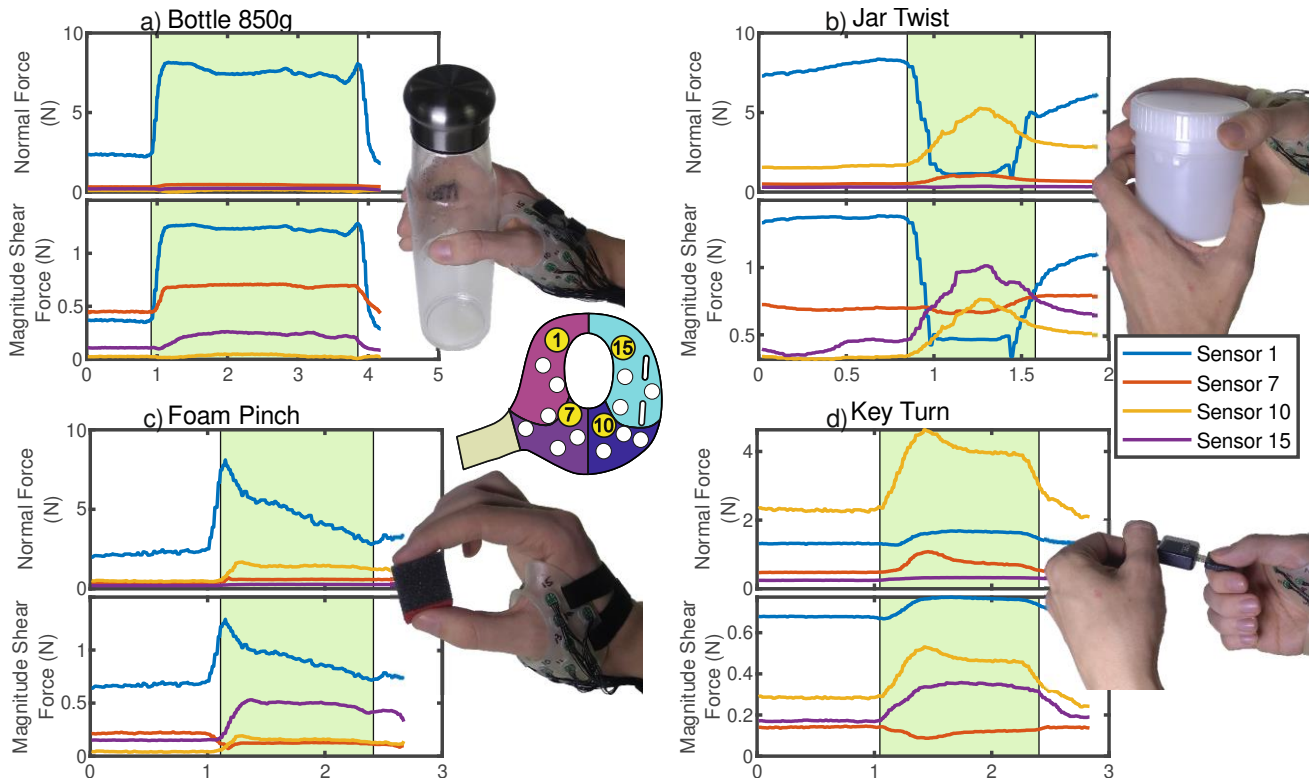 and splint, participants were asked to use only their fingers to grasp the bottle, leaving a gap between the bottle and palm. A High-Density Polyethylene jar with a Polypropylene lid (diameter 83 mm) was used for the jar twist. Participants were asked to hold the jar body in their left hand while twisting the lid in their right. The tripod and pinch grips were tested on a 30 × 30 × 30 mm foam cube (Standard Sheet, Shadow Foam Ltd, UK). The foam was held in the specified fingers and then fully compressed, held for two seconds, and released. The key turn was performed on a 30 mm wide, 59 g padlock (131D, Masterlock, WI, USA). Participants were asked to grip the key in a lateral pinch and turn the key 90° in the lock, held for 1 second, and then return to the initial position.

Data were recorded from the prototype at 100 Hz using the attached microcontroller (Teensy 3.6, PJRC, OR, USA) and sent via USB to a custom LabVIEW script (National Instruments, TX, USA) for data storage and visualisation. Data were saved in a tab-delimited text (.txt) file and stored in an encrypted Cloud Drive (Onedrive for Business, Microsoft, NM, USA). No participant identifying data was stored. Data were post-processed using Matlab to generate statistical data and figures. The results of typical measurements during each task type are presented in Fig. 5. To effectively analyse the results, two means were generated from the data: a baseline mean of the forces when the hand was in 'its functional position but not active (F_{base}), and an active value when the task was performed (F_{task}, green areas, Fig. 5.). This allowed for a task-specific

comparison of activation, independent of the hand posture. To define the active state of the hand, a resistive film pressure sensor (Flexiforce, TekScan, MA, USA) was placed between the thumb and grasped object. Activity was defined as when the thumb contact force was greater than 1 N. To focus the analysis and locate the active areas of the splint, an activation metric was calculated for each sensor based on the magnitude of all three component forces, shown in equation 4.

$$Activation = \frac{\|\boldsymbol{F}_{task}\|}{\|\boldsymbol{F}_{base}\|} - 1 \qquad (4)$$

The activation metric allows for a comparison of the forces during the tasks while negating the effects of the initial force, which may be affected by factors such as the initial tightness of the splint. An example of the activation of each node is presented in Fig. 4e. These metrics were then mapped onto a splint schematic based on the magnitude of activation.

III. RESULTS

A. Comparison of Commercial and 3D Printed Splint Prototypes

The results of the comparison between commercial and 3D printed splints are presented in Fig. 6; a paired sample t-test showed no significant differences in the baseline fit of the splints ($p > 0.05$) and thus indicating that the 3D printed splint has a similar 'fit' to the commercial splint. In the tripod grip task, there was no significant difference in force for sensor 7 ($p > 0.05$), while sensors 1, 10, and 15 showed significant differences ($p < 0.001$) but similar characteristics of low loading. Overall, sensor forces during baseline fit were similar for both splints, and while forces were apparently different
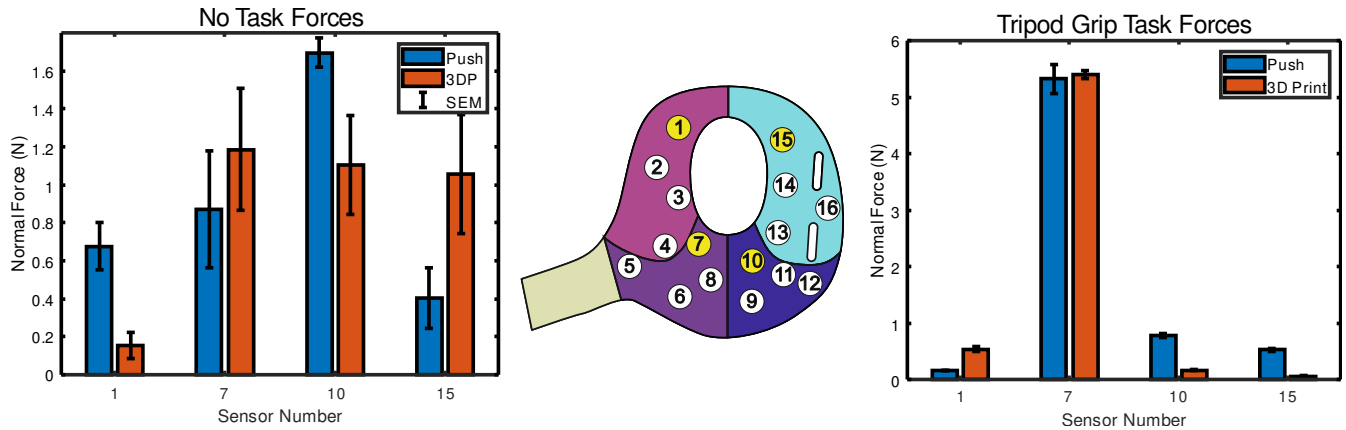
Fig. 6. a)Resting forces comparison between the 3D Printed and Commercial prototypes, b) The shared sensor locations between the prototypes, indicated in yellow; c) Observed mean sensor forces between the prototypes in a tripod grip.

during an active task, the most extreme forces were comparable and the pattern of force distribution was comparable.

B. 3D Printed Splint Pilot Study

All participants completed the study successfully and without any adverse events occurring. All data were successfully recorded and analysed as proposed across the range of functional tasks. Fig. 4d presents the mean values of splint fit across all participants. Seven nodes present with higher loading than others, which all fall around an anatomical landmark. Sensors 8, 9, and 10 fall around the proximal end of the first metacarpal bone and the CMC1 joint. Sensors 1, 2, and 13 sit around the distal end of the metacarpal bone and the MCP1 joint. These areas typically have a lower level of soft tissue coverage and will experience a lower level of force dissipation in the interface.

Fig. 5 presents typical force traces from each of the four task groups: Bottle lifts, Jar Twist, Key Turn, and Foam Pinch. In the bottle tasks, force increases as the bottle is lifted, keeps constant while held, and then decreases to the baseline when released. In the jar twist, forces rise while the jar is gripped and begun to turn, peaking as the lid begins to release. As the jar lid

turns, forces ramp down to the baseline level. In the foam pinch, the forces quickly peak as the foam is compressed before slowly ramping down toward the baseline as the foam is held. When fully released, the forces return to the baseline level. The forces begin to rise slightly before the activity is sensed, owing to the compliant nature of the foam not activating the thumb sensor as movement begins. In the key turn, forces quickly rise to a peak as the key is turned before decreasing to a plateau as the key is held. As the key is released, forces return to the baseline level.

Fig. 7 presents the mean forces observed in the active portion of each task across all participants. Across all tasks, forces are similar but slightly higher than those observed in the baseline fit. In each task type, different areas of the splint exhibit higher forces primarily focused around the ends of the metacarpal bone. In the bottle lifts, the highest forces come from sensors 1, 2, and 13. This highlight support at the distal end of the metacarpal bone. The forces in sensors 1 and 2 are highest, indicating that more support is given to the palmar side of the bone. In the Foam pinch, sensors 9 and 13 show the biggest change. These sensors sit at either end of the metacarpal bone, on its dorsal side, indicating the splint assisting the forces
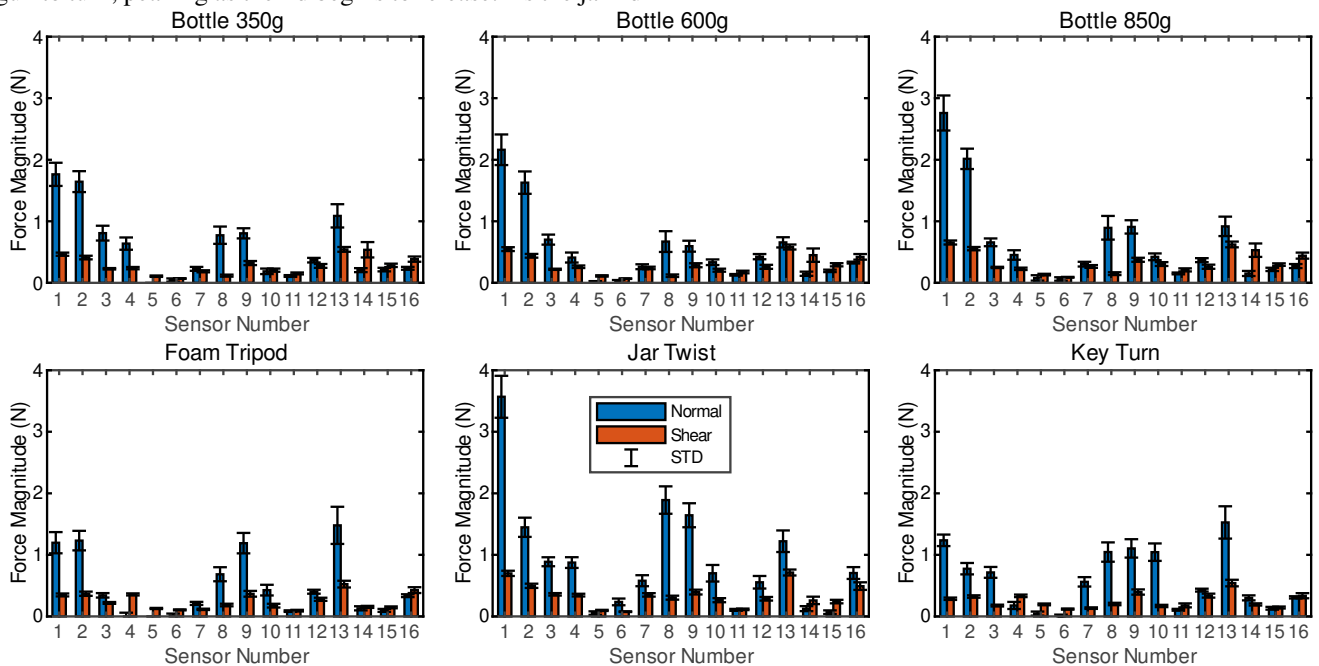

Fig. 7. Force results from the healthy trial. Mean forces ± STD are indicated for each sensor and task.

through the thumb. The jar twist shows the highest forces in the trial, with peaks at sensors 1, 8, 9, and 13. As before, this indicates assistance from the splint, but the high forces in senor one indicate either localised pressure as the splint is pushed into the palmar side of the thumb or could be an artefact of accidental contact between the splint and jar. The key turn has high forces at sensors 8, 9, and 13, once again indicating areas of pressure on the dorsal metacarpal bone.

Fig. 8 presents a summary of the activation schematics, grouped by task type. Each of the functional tasks shows a distinct 'activation area', indicating a significant change in force between the passive and active states of the hand when completing the task. For the pinch tasks, the activation focuses predominantly on the proximal regions of the thumb, with the highest activation seen at senor 8 adjacent to the CMC1 joint.

For the bottle lifts, the activation is more widespread and lower in magnitude, with a minor focus on the proximal areas. High activation is also seen in sensor 1, indicating either mechanical support of the MCP1 joint or accidental contact with the bottle. As the bottle weight is increased, the activation percentage also increased. The key turn activation shows a high activation around the CMC1 joint and proximal end of the metacarpal bone at sensors 8, 9, and 10. For the Jar Twist, activation is both higher and more widespread than the other tasks owing to the wider grasp required to complete the task. The highest activations are observed on the distal regions of the thumb, indicating that the contact is focused around the support of the MCP1 joint.
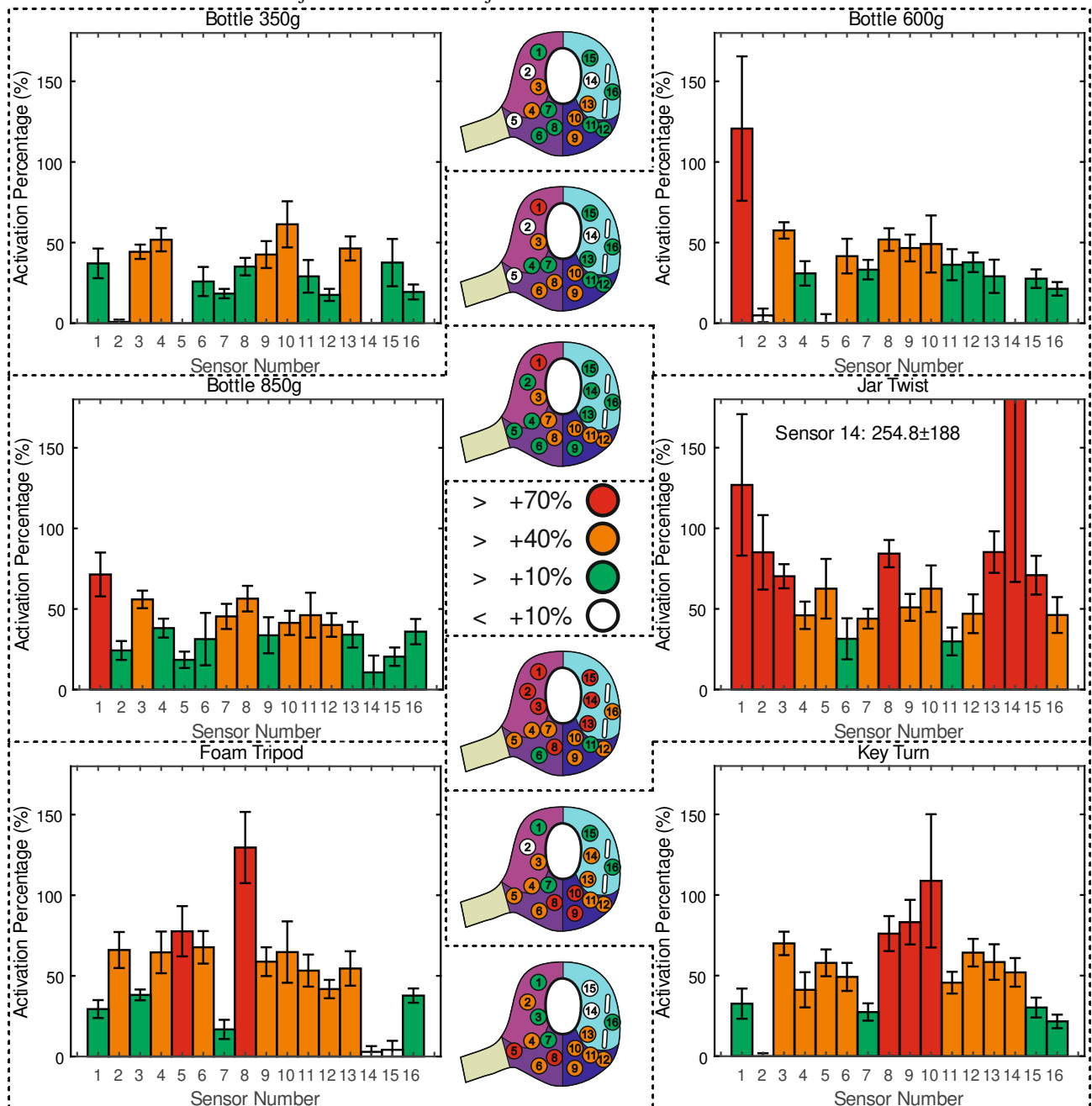

Fig. 8. Activation results from the healthy trial. Areas of greater than 60% activation are indicated in red, 30% in orange, and 10% in green. Activations of lower than 10% are not coloured.

IV. DISCUSSION

The HAILO splint is a proof of concept device intended for the measurement of contact and shear forces between the hand and a thumb splint. It offers a currently unique insight into the function of these devices. The contact and shear forces are measured across the splint-skin interface by an array of sixteen three-axis force sensing nodes.

The initial comparison of the commercial hand splint and 3D printed replica showed similarity in measured forces during baseline fit and similarity in overall force pattern during an active task. However, the forces were shown to be significantly different in the nodes with lower force on the active task. In particular, the sensor on the palmar side of the hand indicated higher forces in the 3D printed splint, while those on the dorsal side were shown to be lower. This was deemed to be caused by the difference in materials between the splints. The commercial splint was made of a low stiffness thermoplastic, while the 3D printed version was made from a stiffer UV cure resin. This variance in force was caused by lower deformation in the stiffer 3D printed splint, as the primary motion of the thumb was toward the palmar side. Despite this, the 3D printed splint still gives a good insight into where high forces are being observed and allows an indication of where future sensing should be focused.

A limitation of the current splint is the variation in baseline contact forces between sessions of wear. In this way, error may be introduced to the system if the splint is initially fitted incorrectly. To remedy this, a preconditioning step was added, where the splint was initially fitted before opening and closing the hand 10 times, allowing the splint to settle onto the hand. The force data recorded indicates that a consistent fit may be achieved between different participants. This opens the avenue for the splint sensing technology to be used as a monitor of the consistent fitment of splints, assisting orthotic technicians in their work. Further analysis may be done in future experimentation to analyse the effect of improper fitting on the function of the splint. This also indicates another potential usage of the force-sensing splint; one could effectively ensure that a splint is fitted correctly by measuring and analysing contact forces across the surface.

In the pilot study involving healthy participants, the splint was shown to vary in response to different activities. By analysing the characteristic response under hand movement, it could be possible to distinguish between different task types. Each task in the experiment followed a standard grip type, with each group exhibiting different biomechanical responses at the base of the thumb. Cylindrical grips, seen in the bottle lift, offer a broad zone of activation across the whole splint surface. In tip grips, seen in the foam squeeze tasks, forces are focused on the proximal thumb, with high activation seen towards the palm as the muscles in the thenar eminence contract. A lateral grip, seen in the key turn, activates around the proximal metacarpal bone. As the key grip causes amplified forces in the CMC joint [9], this shows the splint offering support to the joint. Across the range of tasks, one standout observation was the link between the size of the grasped object and a more even distribution of activation. This indicates a relationship between the fit of the splint and the sensor response: a well-fitting splint would increase contact with the sensors allowing for a more accurate measurement of the interaction. While this study focuses on healthy participants, there is potential for participants with thumb pathologies to have a different degree of motion. To show this, a full biomechanical analysis will be required in future experimentation.

Both the sensor activation and raw force results offer a previously unseen insight into the interactions between the hand and a splint. Across the range of practical tasks, high forces and activations are observed to be mainly localised around the CMC1 and MCP1 joints. For the CMC1 joint, high forces are observed across most tasks. In literature, under many functional tasks the CMC1 joint will sublux and slide out of position. While this is not necessarily present in the healthy population, it is likely to be seen in pathological thumbs. For the MCP1 joint, the splint applies greater force in tasks that require the thumb to be in a wide gripping position. This correlates as areas on the thumb that typically have a low level of soft tissue coverage, on which levels of force transmission to the bones will be higher. This highlights a trait of areas that may be more heavily populated with sensors in future versions of the splint to give an improved spatial resolution. While this is true for healthy participants, those presenting with arthritis may exhibit different trends. To ensure that these are taken into account, a clinical trial will be needed to assess these forces and advise future design.

While this research focuses on a custom 3D printed instrumented splint, we have shown that we have the ability to incorporate sensors within a commercial "off the shelf" model. With no further adaptation, these sensors could be incorporated within a wide variety of splints in a clinical setting, both other commercial splints and custom clinic models. The current sensor configuration is specified for the expected force interactions with the hand but could also be tuned for applications with greater loads, such as those seen in prosthetic sockets.

V. CONCLUSION

In this paper, sixteen three-axis soft force sensors were integrated into a thumb spica splint. The 3D printed sensorised splint was validated against a commercial splint of similar geometry. A novel calibration approach was used to calibrate the sixteen sensors to account for manufacturing error. The splint was shown to effectively measure contact and shear forces across the splint through a series of everyday tasks. The splint was then used to collect a set of pilot data across a variety of functional hand tasks, indicating the capability of the device to be used in a larger-scale research trial. In particular, the device indicated the ability to detect differing grasping motions. Such a device could be used as a tool to investigate the biomechanical effects of splinting on arthritic hands.

APPENDIX

A. Participant Information:

Testing was undertaken in 5 experiments with each stage taking under 10 mins. This time included time for the initial fitting of the splint. The prototype splint was fitted to the 'participant's right hand. Each experiment was repeated 5 times.

1) Stage 1: Pick Up/ set down cylinder

Participants were asked to pick up and set down a 350, 600, and 850g bottle 5 times for each case.

The bottle was placed in the working area.

For 600g, the bottle was filled with water to the first line. For 850g, the bottle was filled to the second line.

2) Stage 2: Unscrew Jar Lid

Participants were asked to unscrew and tighten a jar lid with their right hand only, 5 times. The jar body was held in the left hand. The jar lid was closed and the body held in the left hand above the working area

3) Stage 3: Key Turn

Participants were asked to turn a key in a padlock clockwise 90deg, and anticlockwise 90deg 5 times. The padlock body was held in the left hand above the working area.

4) Stage 4: Foam Squeeze

Participants were asked to squeeze a foam cube with two different grips: pinch, and tripod grips. The foam was held in the selected grip above the working area.

REFERENCES

[1] L. Xu, R. J. Strauch, G. A. Ateshian, R. J. Pawluk, V. C. Mow, and M. P. Rosenwasser, "Topography of the osteoarthritic thumb carpometacarpal joint and its variations with regard to gender, age, site, and osteoarthritic stage," *J. Hand Surg. Am.*, vol. 23, no. 3, pp. 454–464, 1998.

[2] M. M. Haara *et al.*, "Osteoarthritis in the carpometacarpal joint of the thumb: prevalence and associations with disability and mortality," *JBJS*, vol. 86, no. 7, pp. 1452–1457, 2004.

[3] A. L. Armstrong, J. B. Hunter, and T. R. C. Davis, "The prevalence of degenerative arthritis of the base of the thumb in post-menopausal women," *J. Hand Surg. Am.*, vol. 19, no. 3, pp. 340–341, 1994.

[4] Y. Zhang, J. Niu, M. Kelly-Hayes, C. E. Chaisson, P. Aliabadi, and D. T. Felson, "Prevalence of symptomatic hand osteoarthritis and its impact on functional status among the elderly: The Framingham Study," *Am. J. Epidemiol.*, vol. 156, no. 11, pp. 1021–1027, 2002.

[5] R. W. Hwang and D. Ring, "Pain and disability related to osteoarthrosis of the trapeziometacarpal joint," *J. Hand Microsurg.*, vol. 3, no. 02, pp. 63–65, 2011.

[6] K. S. Matullo, A. Ilyas, and J. J. Thoder, "CMC arthroplasty of the thumb: a review," *Hand*, vol. 2, no. 4, pp. 232–239, 2007.

[7] K. O. Cho, "Translocation of the abductor pollicis longus tendon: a treatment for chronic subluxation of the thumb carpometacarpal joint," *JBJS*, vol. 52, no. 6, pp. 1166–1170, 1970.

[8] V. D. Pellegrini Jr, "The ABJS 2005 Nicolas Andry Award: Osteoarthritis and injury at the base of the human thumb: survival of the fittest?," *Clin. Orthop. Relat. Res.*, vol. 438, pp. 266–276, 2005.

[9] J. C. Colditz, "The biomechanics of a thumb carpometacarpal immobilization splint: design and fitting," *J. Hand Ther.*, vol. 13, no. 3, pp. 228–235, 2000.

[10] E. J. Otten, *Roberts and Hedges Clinical Procedures in Emergency Medicine*, vol. 40, no. 4. 2011.

[11] J. U. Poole and J. V. D. Pellegrini, "Arthritis of the thumb basal joint complex.," *J. hand Ther. Off. J. Am. Soc. Hand Ther.*, vol. 13, no. 2, pp. 91–107, 2000.

[12] J. Tsehaie *et al.*, "Predicting Outcome After Hand Orthosis and Hand Therapy for Thumb Carpometacarpal Osteoarthritis: A Prospective Study," *Arch. Phys. Med. Rehabil.*, vol. 100, no. 5, pp. 844–850, May 2019, doi: 10.1016/j.apmr.2018.08.192.

[13] M. Buhler, C. M. Chapple, S. Stebbings, B. Sangelaji, and G. D. Baxter, "Effectiveness of splinting for pain and function in people with thumb carpometacarpal osteoarthritis: a systematic review with meta-analysis," *Osteoarthritis and Cartilage*, vol. 27, no. 4. W.B. Saunders Ltd, pp. 547–559, Apr. 01, 2019, doi: 10.1016/j.joca.2018.09.012.

[14] F. Rannou *et al.*, "Splint for base-of-thumb osteoarthritis: a randomized trial," *Ann. Intern. Med.*, vol. 150, no. 10, pp. 661–669, 2009.

[15] M. Arazpour *et al.*, "The effect of thumb splinting on thenar muscles atrophy, pain, and function in subjects with thumb carpometacarpal joint osteoarthritis," *Prosthet. Orthot. Int.*, vol. 41, no. 4, pp. 379–386, 2017.

[16] A. C. G. Carreira, A. Jones, and J. Natour, "Assessment of the effectiveness of a functional splint for osteoarthritis of the trapeziometacarpal joint on the dominant hand: a randomized controlled study," *J. Rehabil. Med.*, vol. 42, no. 5, pp. 469–474, 2010.

[17] J. Adams *et al.*, "The clinical and cost effectiveness of splints for thumb base osteoarthritis: a randomized controlled clinical trial," *Rheumatology*, Nov. 2020, doi: 10.1093/rheumatology/keaa726.

[18] M. Buhler, C. M. Chapple, S. Stebbings, J. Adams, D. Gwynne-Jones, and G. D. Baxter, "Splinting for thumb carpometacarpal osteoarthritis: protocol for a feasibility randomized controlled trial," *Phys. Ther. Rev.*, pp. 1–9, May 2020, doi: 10.1080/10833196.2020.1763662.

[19] R. B. Giesberts, A. M. ter Haar, G. M. Sanderman, E. E. G. Hekman, and G. J. Verkerke, "Tissue adaptation rate in the treatment of Dupuytren contracture," *J. Hand Ther.*, 2019.

[20] R. Giesberts, V. Sluiter, and G. Verkerke, "Design and test of a new inductive force sensor," *Sensors*, vol. 18, no. 7, p. 2079, 2018.

[21] X. Tan, L. He, J. Cao, W. Chen, and T. Nanayakkara, "A Soft Pressure Sensor Skin for Hand and Wrist Orthoses," *IEEE Robot. Autom. Lett.*, vol. 5, no. 2, pp. 2192–2199, Apr. 2020, doi: 10.1109/LRA.2020.2970947.

[22] C.-C. Tuan *et al.*, "Development of a System for Real-Time Monitoring of Pressure, Temperature, and Humidity in Casts," *Sensors*, vol. 19, no. 10, p. 2417, 2019.

[23] S. Laufer *et al.*, "Sensor-based assessment of cast placement and removal," *Stud. Health Technol. Inform.*, vol. 196, p. 259, 2014.

[24] E. A. Al-Fakih, N. A. Abu Osman, and F. R. Mahmad Adikan, "Techniques for interface stress measurements within prosthetic sockets of transtibial amputees: A review of the past 50 years of research," *Sensors (Switzerland)*, vol. 16, no. 7. MDPI AG, Jul. 20, 2016, doi: 10.3390/s16071119.

[25] S. Gupta, K. J. Loh, and A. Pedtke, "Sensing and actuation technologies for smart socket prostheses," *Biomedical Engineering Letters*, vol. 10, no. 1. Springer Verlag, pp. 103–118, Feb. 01, 2020, doi: 10.1007/s13534-019-00137-5.

[26] S. Ugolini *et al.*, "Sensorized Orthosis for Non-Operative Treatment of $Pectus~Carinatum$ in Pediatric Patients," *IEEE Trans. Med. Robot. Bionics*, vol. 1, no. 2, pp. 115–121, May 2019, doi: 10.1109/tmrb.2019.2913709.

[27] L. Wang *et al.*, "A Review of Wearable Sensor Systems to Monitor Plantar Loading in the Assessment of Diabetic Foot Ulcers," *IEEE Trans. Biomed. Eng.*, pp. 1–1, Dec. 2019, doi: 10.1109/tbme.2019.2953630.

[28] R. Eguchi, A. Yorozu, T. Fukumoto, and M. Takahashi, "Estimation of Vertical Ground Reaction Force Using Low-Cost Insole with Force Plate-Free Learning from Single Leg Stance and Walking," *IEEE J. Biomed. Heal. Informatics*, vol. 24, no. 5, pp. 1276–1283, May 2020, doi: 10.1109/JBHI.2019.2937279.

[29] L. Wang *et al.*, "Design of a Digital Triaxial Force Sensor for Plantar Load Measurements," 2019, doi: 10.1109/SENSORS43011.2019.8956606.

[30] S. Roy, S. S. Mathew-Steiner, and C. K. Sen, "Residual Limb Health and Prosthetics," in *Prosthesis*, IntechOpen, 2020.

[31] D. Popescu, A. Zapciu, C. Tarba, and D. Laptoiu, "Fast production of customized three-dimensional-printed hand splints," *Rapid Prototyp. J.*, vol. 26, no. 1, pp. 134–144, Jan. 2020, doi: 10.1108/RPJ-01-2019-0009/FULL/HTML.

[32] D. Jones *et al.*, "Design and Evaluation of Magnetic Hall Effect Tactile Sensors for Use in Sensorized Splints," *Sensors*, vol. 20, no. 4, p. 1123, Feb. 2020, doi: 10.3390/s20041123.

[33] H. Wang *et al.*, "Design methodology for magnetic field-based soft tri-axis tactile sensors," *Sensors*, vol. 16, no. 9, p. 1356, 2016.

[34] L. Wang *et al.*, "An Inductive Force Sensor for In-Shoe Plantar Normal and Shear Load Measurement," *IEEE Sens. J.*, pp. 1–1, 2020, doi: 10.1109/JSEN.2020.3006316.